



# Multidirectional 3D-printed functionally graded modular joint actuated by TCP<sub>FL</sub> muscles for soft robots

Armita Hamidi<sup>1</sup> · Yara Almubarak<sup>1</sup> · Yonas Tadesse<sup>1</sup> 

Received: 20 August 2019 / Accepted: 24 October 2019  
© Zhejiang University Press 2019

## Abstract

Highly deformable bodies are essential for numerous types of applications in all sorts of environments. Joint-like structures comprising a ball and socket joint have many degrees of freedom that allow mobility of many biomimetic structures. Recently, soft robots are favored over rigid structures for their highly compliant material, high-deformation properties at low forces, and ability to operate in difficult environments. However, it is still challenging to fabricate complex designs that satisfy application constraints due to the combined effects of material properties, actuation method, and structural geometry on the performance of the soft robot. Therefore, a combination of a rigid joint and a soft body can help achieve modular robots with fully functional body morphology. Yet, the fabrication of soft parts requires extensive molding for complex shapes, which comprises several processes and can be time-consuming. In addition, molded connections between extremely soft materials and hard materials can be critical failing points. In this paper, we present a functionally graded 3D-printed joint-like structure actuated by novel contractile actuators. Functionally graded materials (FGMs) via 3D printing allow for extensive material property enhancement and control which warrant tunable functionalities of the system. The 3D-printed structure is made of 3 rigid ball and socket joints connected in series and actuated by integrating twisted and coiled polymer fishing line (TCP<sub>FL</sub>) actuators, which are confined in the FGM accordion-shaped channels. The implementation of the untethered TCP<sub>FL</sub> actuation system can be highly beneficial for deployment in environments that require low vibrations and silent actuation. The fishing line TCP actuators produce an actuation strain up to 40% and bend the joint up to 40° in any direction. The TCP<sub>FL</sub> can be actuated individually or as a group to control the bending trajectory of the modular joint, which is beneficial when deployed in areas that contain small crevices. Obtaining complex modes of bending, the FGM multidirectional joint demonstrated a great potential to achieve different functionalities such as crawling, rolling, swimming, or underwater exploration.

**Keywords** Functionally graded · 3D-printed · Joint · Multidirectional · Fishing line TCP

---

Armita Hamidi and Yara Almubarak have equal contribution for this work.

---

**Electronic supplementary material** The online version of this article (<https://doi.org/10.1007/s42242-019-00055-6>) contains supplementary material, which is available to authorized users.

---

✉ Armita Hamidi  
armita.hamidi@utdallas.edu

<sup>1</sup> Humanoid, Bio-robotics and Smart Systems (HBS) Laboratory, Mechanical Engineering Department, The University of Texas at Dallas, Richardson, TX 75080, USA

## Introduction

Recently, functionally graded materials (FGMs) are taking the lead over composite bulk materials due to the variation of their properties such as elastic modulus, stiffness, and extent of deformation. The smooth transition of material's stiffness gradient and controlled mechanical properties eliminates the drawbacks of conventional composites such as interface problems [1]. Delamination or failure of components is one of the problems that generally occur in a region where there is a sharp transition of material properties, especially at the joints and linkages. Weak bonding is another problem at an interface between dissimilar materials. FGMs can create stronger bonds and reduce residual and thermal stresses by eliminating material discontinuities [2]. Many biological systems have FGM architecture, which is an integration of

rigid materials such as teeth or bone [3] into soft tissues to achieve optimum performance. The combination of muscles, bones, cartilages, and ligaments in the musculoskeletal system is one of the natural examples of FGM structures. For example, Monzon et al. [4] discussed the capabilities of FGM for building scaffolds that can be implanted directly in human body for osteoarthritis treatment. In animals, the angle and compliance of the joint for bending are directly dependent and controlled by the muscles surrounding it [5]. Zhang et al. [6] and Ji et al. [7] discussed the utilization of 3D printing in tissue engineering for developing cartilage, bone, and skin, but it is still challenging to combine all of these parts to construct an organ with required functionality by a single fabrication process, i.e., combination of bone and cartilage in a joint structure. On the other hand, in order to build a system that resembles the tissue structure for robotic applications, the actuator needs to be flexible enough to deform easily within the structure.

To date, many artificial musculoskeletal systems are presented that are controlled by different actuation technologies such as motor-based tendons [8, 9], pneumatic artificial muscles [10–13], and twisted and coiled polymer (TCP) muscles [14, 15]. Complicated actuation systems such as electrical motors ranging from stepper to servo and air/water supply units in pneumatic/fluidic actuators limit the size and space of the bioinspired design [10], making it inconveniently bulky, heavy, and expensive. Therefore, the research is ongoing for developing new actuators or actuation mechanisms to power soft robots. For instance, Robertson and Paik [16] developed a foam-based vacuum-powered actuator that has multiple degrees of freedom (DOF). They showed different functions including multimodal locomotion, gripping, and stiffening through granular media jamming, which could be accomplished by combining these vacuum-powered modules. In another study [17], a tendril-like soft robot based on the osmotic actuator (the electrosorption of ions on flexible electrodes) is presented. It was demonstrated that this plant-shaped soft robot can achieve a reversible increase in bending stiffness by increasing the power, although it takes a relatively higher actuation time (1 hour) compared to other methods.

Shape memory alloys (SMAs), dielectric elastomers (DEs), and twisted and coiled polymer actuators (TCPs) are other popular actuators for use in soft robots, since they can be easily inserted or embedded into the soft structures. The ability to obtain multiple independently controlled channels can be used in many applications that need multi-DOF systems such as finger joint in prosthetic hands [18]. Ransley et al. [19] 3D-printed a chainmail fabric structure that included several individual solid links containing NiTi coils nested within a spring steel. The structure contracted when actuated and transformed from a curved drape profile to a rigid cantilever.

Regarding new polymeric muscles, TCPs are developed by Haines et al. [20] by coiling inexpensive high-strength polymer fibers after extreme twist insertion. Almubarak and Tadesse [21] obtained different soft morphed structures by embedding these TCP actuators in soft silicone skins with different thicknesses and actuating them at different input power. Wu et al. [22] designed and developed a single musculoskeletal joint actuated by TCP artificial muscles fabricated from fishing line and nichrome wire. They used silicone molding and multistep assembly to form channels around a rigid 3D-printed ball and socket joint and inserted TCPs in them. Recently, Tang et al. [23] have also used the same principle and presented a simple soft crawling structure by embedding TCPs in silicone. They also developed a soft robotic module using 3 TCP actuators placed through channels inside a cast silicone in another work [24]. This robotic module was controlled based on a temperature feedback control system. However, they mentioned some problems in the trajectory control of the structure when the muscles are actuated such as slow response due to the very long time required for complete cooling of the TCP, and limited bending angle due to the rigidity of the whole body.

One of the important aspects related to the functionality of a soft robot is the adaptation to the working environment based on the application. An integrated design with appropriate selection of materials, actuators, and control system can effectively make the soft robots highly capable. The key challenges are movement and stiffness modulation, which are both required for an effective demonstration and control. Nowadays, modulation or control of the stiffness is essential in soft robots [25]. For instance, Bartlett et al. [26] presented a 3D-printed functionally graded robot that can autonomously jump a height up to 0.76 m and demonstrated horizontal jumping up to 0.15 m distance. The stiffness gradient provided the necessary rigidity to transfer the impulse of combustion to generate effective jumping, and the compliance of the base absorbed and dissipated the energy of the landing impact.

The motivation of our work is to create a bioinspired joint that eliminates constraints such as manual assembly, actuation system, and control of a robotic structure with multiple joints. In this regard, we presented the design, fabrication, and characterization of a modular cascaded joint powered by electrically driven self-coiled fishing line TCP actuators (Fig. 1). By taking advantage of multimaterial 3D printing technology, tuning the structural properties and the geometry that is suitable for the soft actuator, we were able to create different actuation modes. Therefore, a full characterization on self-coiled fishing line TCP with nichrome heating wire ( $TCP_{NC}^{FL}$ ) actuators is also performed. Moreover, a circuit is designed and developed to control the robot wirelessly via Bluetooth. Finally, we have shown that a combination of fishing line TCP muscles and the modular 3D-printed joint

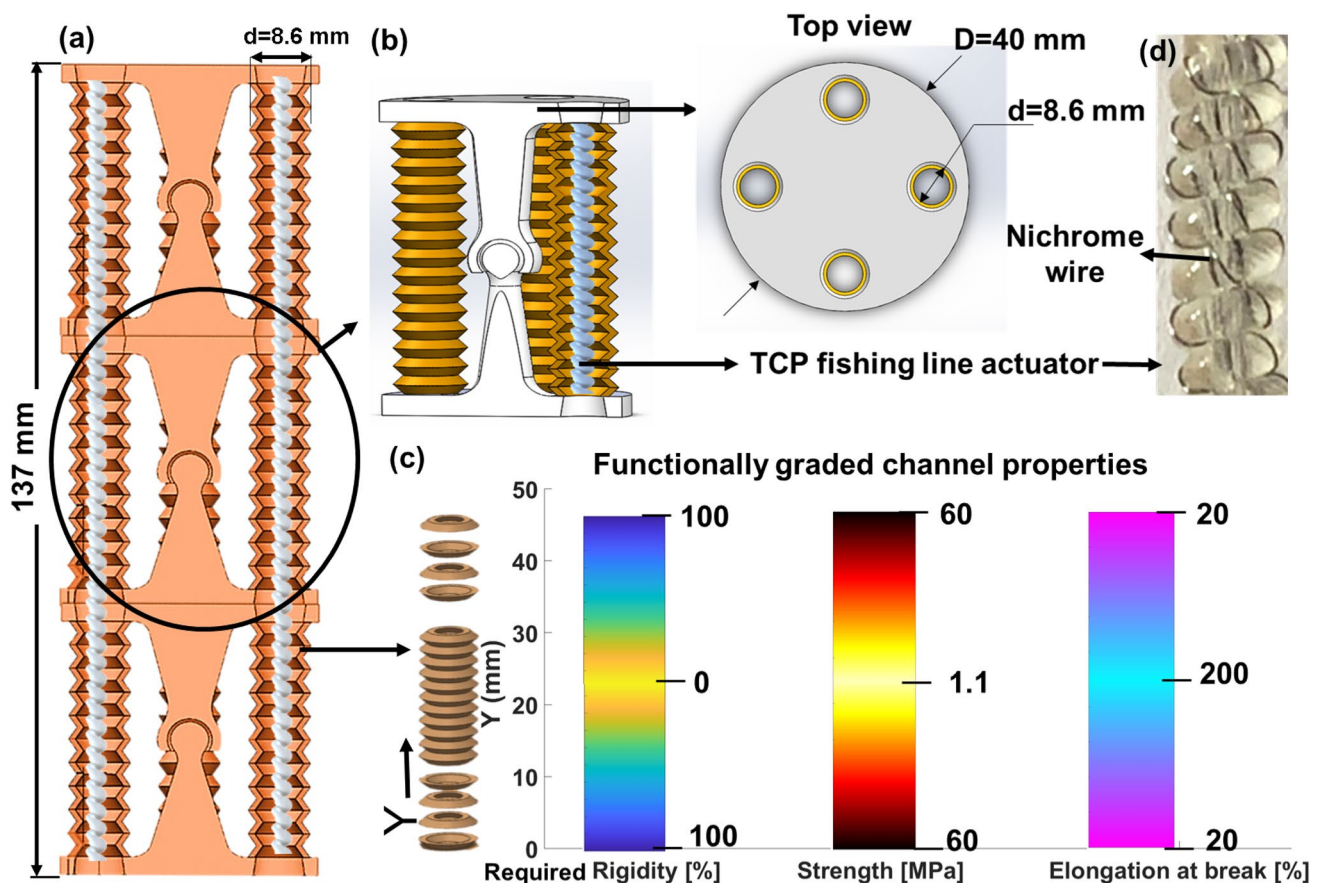


**Fig. 1** Functionally graded joint, **a** cascaded joints structure design, **b** functionally graded properties of the channel along with the height, and **c** the detailed joint structure and dimensions and **d** fishing line TCP with nichrome wire

has many potential applications, such as serving as medical robots, inspection and exploration systems, snake-like robots, underwater manipulators, and underwater swimming robots. The highlights of this work are summarized as follows:

- Employing additive manufacturing through FGM resulted in controlled properties of the structure during fabrication. Setting the desired properties at specific components and locations without long procedures of fabrication or step-by-step assembly of a complicated structure is the most significant improvement of using this method to achieve the targeted bioinspired design.
- Self-coiled fishing line TCP with nichrome heating wire, with an overall diameter of 2.8 mm, is characterized using three types of actuation methods: slow, fast, and sequential actuation. Maximum actuation strains up to 40% of its original loaded length is achieved at 300 g load at 0.16 A current input with 20 s heating time (slow actuation, 16% duty cycle).
- Untethered actuation of the robotic structure is demonstrated via a battery-powered circuit module consisting

of wireless communication, switches, Arduino board, voltage boost converter, and a laptop as a base station.

- The tuneable functionalities and various deformations of the presented musculoskeletal system can be used for many applications in a wide range of fields.

## Materials and methods

### Design and development of FGM joint

Taking inspiration from animalistic structures found in nature and the work presented by Wu et al. [22], a system of three cascaded joints is designed and created as shown in Fig. 1a. A multimaterial 3D printer (Objet350 Connex3, Stratasys) is used to directly print the functional body of the robot by a single attempt and eliminating the need for complex casting and molding techniques or assembly. The three joints consist of ball and socket joints between two bone-like structures that are also surrounded by four hollow channels (8.6 mm diameter) (Fig. 1b). This design allows users to take advantage of a wide range of motions

(abduction–adduction, flexion–extension, and circumduction) due to the rotational degree of freedom of the ball and socket design. FGM 3D printing can enhance the mechanical properties of the structures and implementation of bioinspired design concepts. The ball and socket joint is printed by a rigid material (Veroclear, tensile strength of 50–65 MPa, 83–86 shore scale D [27]), and the channels are printed by a stepwise gradient of nine different layers, creating a structure that transitions from fully rigid (thermoplastic-like) to highly flexible (rubber-like) soft material (TangoPlus, elongation at break of 218% and 27 shore scale A [27]). A range of mechanical properties can be achieved by combining different materials at high resolution as shown in other works [28, 29]. By digitally combining two different materials, we are able to build the functionally graded channels. Each channel is divided into 9 equal segments from top to bottom, each 2.2 mm in length. Then, different ratios of soft and rigid material were assigned to each segment. The top and bottom of the channels are 3D-printed by 100% rigid material, and the next layer is 90% rigid material combined with 10% soft material. This order continues until the middle section reaches 100% soft material. The stiffness of the four channels is changed from softest at the center to the stiffest at the connection spots with the end flanges as shown in Fig. 1c. The accordion channel design with a 1-mm thickness and the stiffness gradient provided a good bending deformation of each channel. If thinner smooth cylindrical channels were used within this design, the material would simply fail when the channels are deformed. Overall, the center, top, and bottom caps of the joint made by this method have the highest stiffness, the same as the one presented by Wu et al. [30], while the channels in this work are functionally graded and soft enough to bend. For the driving component, four self-coiled fishing line TCP actuators coiled with nichrome wire (Fig. 1d) are arranged in a symmetrical manner about the circumference of the FGM 3D-printed structure. The TCP<sub>FL</sub> actuator fabrication and characterization for driving the joints are described in the following section.

### Self-coiled fishing line with nichrome wire TCP<sub>FL</sub><sup>NC</sup> actuator fabrication and characterization

The fabrication of the actuator (general information found in Table 1) was conducted following the work process introduced in [22]. It consists of several simple steps as shown in Fig. 2a. First, a twist is inserted into the precursor fiber. The precursor fishing line ( $d=0.8$  mm,  $L=1100$  mm) is connected to a motor on the one end and a stopper on the other end, keeping the fiber in tension using 500-g load. The motor is activated to rotate counterclockwise to fully incorporate a twist into the fiber. Once the fiber starts coiling

**Table 1** Self-coiled fishing line actuator information

Material	Nylon (6,6) fishing line
Type of actuation	Electrothermal
Type of resistance wire	Nichrome (nickel, chromium)
Resistance wire diameter	$d_w=80$ $\mu$ m
Precursor fiber diameter	$d=0.8$ mm
Length of precursor fiber	$l=1100$ mm
Weight for fabrication	$m_f=500$ g
Annealing temperature/time	$T_a=180$ °C/90 min
Diameter after coiling	$D=2.8$ mm
Length after coiling	$L=170$ mm
Resistance	$R=360$ $\Omega$
Current (input)	$I=0.16$ – $0.32$ A
Voltage (output)	$V=57.6$ – $115.2$ V
Actuation power	$P=9.2$ – $36.8$ W
Heating time	$t_h=20$ – $1$ s
Cooling time	$t_c=100$ – $9$ s
Heating energy	$E_h=184.32$ – $36.8$ J
Actuation frequency	$f=0.16$ – $0.1$ Hz
Actuation strain, at 300-g load	$\epsilon=38$ – $10\%$
Blocking force	$F_b=800$ g
Life cycle	2400 cycles in air at 9 mHz and 1% duty cycle, expected to have similar lifecycle as in [22]

(fully twisted), the motor is stopped. The second step is adding the nichrome wire. Here, the nichrome wire ( $d_w=80$   $\mu$ m) is incorporated using a rod that controls the pitch of the wire. In order to fully incorporate nichrome without coiling the tensioned precursor fiber, the stopper is removed, allowing the fishing line to untwist partially. Once the wire is fully integrated throughout the length of the precursor, the third step of coiling can begin by adding the stopper again. After coiling, the fishing line is crimped on both ends and annealed in an oven for 90 minutes at 180 °C. The annealing process helps the newly fabricated actuator permanently retain its coiled shape. The final step of the fabrication process is the training phase. The muscle is actuated with the desired load until it reaches steady-state actuation cycles.

The development of new actuators requires extensive experimentation in various scenarios to understand their performance and application capabilities. Experimental characterization of the fabricated TCP actuators based on fishing line was conducted (loaded length  $L=190$  mm, diameter  $D=2.8$  mm, resistance  $R=360$   $\Omega$ ). The experimental setup and schematics are shown in Fig. 2b. The experimental setup includes the fishing line actuator fixed on one end and connected to a slider and calibrated weight on the other end. A Keyence laser displacement sensor is used to measure the actuation strain. Thermocouples and NI DAQ 9219 are used to measure the temperature while actuating. NI DAQ

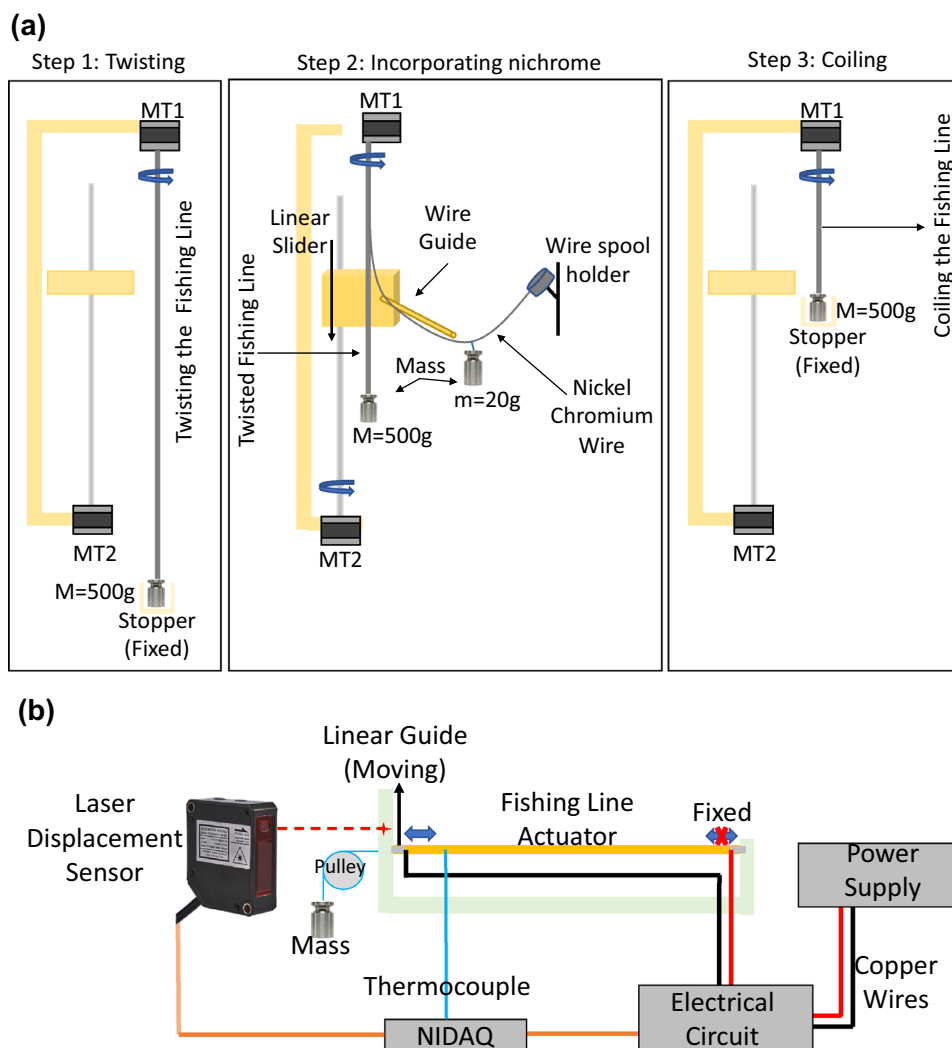


**Fig. 2** Fishing line TCP with nichrome wire: **a** fabrication procedure and **b** isotonic test characterization setup

9221 is used to measure the output voltage due to change of resistance while actuating. A power supply is used to provide constant input current programmed at various time intervals and sequences. The pre-stress parameter was kept at a constant 300-g load. Three tests were conducted each at 3 input current variations. The first test (left green column) examined the actuation in a period of 3 pulses, at 0.12 A, 0.14 A, and 0.16 A input current (each pulse was of frequency  $f=0.16$  Hz, heating time  $t_h=20$  s, cooling time  $t_c=100$  s). Figure 3a shows the cyclic actuation results in which the actuator produces ~ 13%, 24%, and 36% actuation strain at the 0.12 A, 0.14 A, and 0.16 A input currents, respectively. The temperature plot shown in Fig. 3b is an important aspect in studying the actuation behavior of the self-coiled fishing line muscle. It is observed that the increase in temperature results in higher actuation. In general, the results of this experiment highlight the impact of input energy ( $E=VIt=V^2t/R$ , the voltage, current and heating time, and/

or constant resistance) on the performance of the actuator. Data gathered in the experiment indicated that the increase in heating energy will result in an increase in the actuation strain and temperature.

The heat transfer equation presented in Eq. (1) allows us to predict the temperature in relation to several parameters such as the temperature of the actuator  $T(t)$  at time  $t$ , the ambient room temperature  $T_\infty$ , the resistance of the actuator at room temperature  $R_o$ , the input current  $i$ , the cross-sectional area of the precursor fiber of the actuator (nylon)  $A$ , the mass of the actuator  $m$ , the specific heat  $c_p$ , the temperature coefficient for the resistivity  $\alpha$ , the convective heat transfer coefficient  $h$ , and  $t$  which is the heating time:

$$mC_p\dot{T} = i^2R - hA(T - T_\infty) \tag{1}$$

The correlation between the simulated and experimental results helps in reducing the experiments conducted to

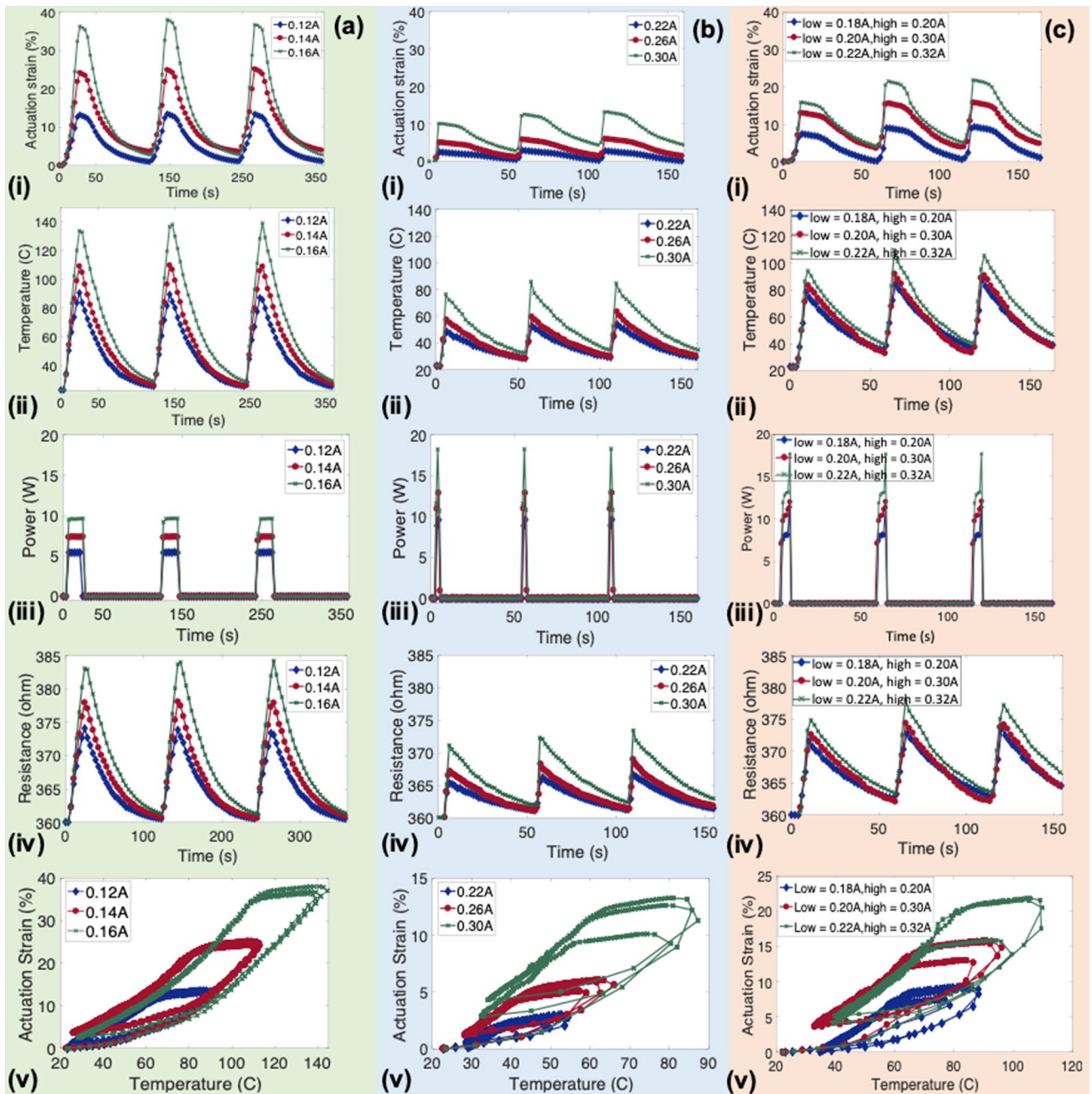


**Fig. 3** Time domain plots of experimental characterization of the self-coiled fishing line. **a** Left: slow actuation of 20-s heating and 100-s cooling. **b** Middle: fast actuation of 2-s heating and 50-s cool-

ing. **c** Right: sequential actuation of 5-s heating and 50-s cooling. (I) Actuation strain. (II) Temperature. (III) Power. (IV) Resistance. (V) Hysteresis

study the actuator and allows the prediction of the maximum actuation parameters (input current, heating time, cooling time) that can be used before the nylon reaches its melting temperature and fail. On the other hand, by assuming that the resistance changes due to the temperature change, Eq. (2) can be used:

$$R(t) = R_0 [1 + \alpha (T(t) - T_\infty)] \quad (2)$$

The temperature coefficient of resistance of the nichrome wire is  $\alpha = 579 \times 10^{-6} \text{ 1/}^\circ\text{C}$  [31]. Figure 3a–c, iii, all results in the fourth row, shows the results of change of the resistance while actuating. These results indicate a significant change caused by the increase of resistance due to the heating and cooling parameters. The increased resistance is a result of the rise in temperature and increased contact between the coils as seen in other studies. The first set of

experiments presented in the far-left column of Fig. 3 show the great strain (40%) potential of the actuator at three different currents at frequency  $f=0.008$  Hz and duty cycle of 16%, (heating time  $t_h=20$  s, cooling time  $t_c=100$  s). Many applications suggested for the presented musculoskeletal design require a fast-compliant mode of actuation rather than higher strain. Therefore, another set of experiments were conducted based on the observations from the previous results. The middle (blue) column presented in Fig. 3 shows the results of 0.22 A, 0.26 A, and 0.30 A input current magnitudes (each pulse was of frequency  $f=0.019$  Hz and duty cycle of 4%, heating time  $t_h=2$  s, cooling time  $t_c=50$  s). The actuator was able to reach an average strain between 2 and 10% as demonstrated in Fig. 3b-i, by reducing the heating time and doubling the input driving power. The general decrease in actuation strain is a result of the reduced heating temperature (Fig. 3b-ii), due to the shorter heating time. Therefore, a third set of experiments are conducted as shown in the right column of Fig. 3 (orange column), which involves stepping the input power at a low heating frequency (3 pulses, two heating and one cooling). The first pulse heating time is  $t_h=4$  s, the second pulse heating time is  $t_h=1$  s, and the last cooling time is  $t_c=50$  s. It is observed that in this case, the actuation strain has increased almost double that of the previous set of tests while still maintaining a fast actuation frequency. According to Fig. 3c-ii, the actuator was able to reach higher temperatures at almost 100 °C compared to Fig. 3b-ii where it only reached a maximum of 80 °C. The balance between increasing the heating temperature and maintaining a practical actuation strain is critical for the functionality of the muscles when heated. While still maintaining the same input power, in the last two sets of experiments (Fig. 3b-ii to c-v), by sequencing the power input into multiple pulses, we are able to achieve almost double the strain by 20 °C increase in temperature. In the three cases, the TCP<sub>FL</sub> does show an increase in hysteresis as the frequency increases. These phenomena can be due to the different factors such as insufficient cooling times, pre-stress loading, input power, and the temperature of the testing environment. Since the actuators are confined in tubes inside the joint structure, heat dissipation while cooling is often slower. Figure 3a–c, v, all the fifth row, shows the three cycle hysteresis plots for low, medium, and high input power for each case. It is observed that in the first case (Fig. 3a-v) a consistent hysteresis of ~20 °C is seen for all the three input currents during the three actuation cycles. For the second case (Fig. 3b-v), it is observed that the hysteresis produced for the lower currents was around 10 °C and 20 °C for the higher input currents. At the higher input currents, there is also a variation between the three cycles as the heat continues to accumulate due to shorter cooling times (for fast actuation). Finally, in the third case, the hysteresis increased to 30 °C for all three input current cases. It is also observed

that the cooling time was insufficient as the number of cycles increases. Several conditions can be conducted to reduce the hysteresis of the actuation, one of which is decreasing the frequency. In all cases, it is observed that as the frequency is increased, the hysteresis is also increased. An ideal situation would be heating the muscle at a slower rate and cooling it down at a slower rate or using forced cooling for increasing the cooling rate. The channels in the modular joints are designed as a provision for cooling of the actuators either by liquid or by cold air, which will be our future work. The purpose of the current work is to study the characteristics at slow actuation and fast actuation, which are associated with the heating time and cooling time.

## Controlling circuit

A circuit was developed to control the joint system with all its components. The circuit consists of a wireless control module, a voltage regulator for muscle activation, and a miniature air pump for forced cooling. An Arduino Uno powered by a 9-V battery is used to control the movement of the structure. Another 14.8-V battery is used to power the two TCP<sub>FL</sub> muscles and the air pump. Relay switches are used to control the TCP<sub>FL</sub> muscles and the air pump. A Bluetooth module (HC-05) is used to wirelessly control the system through a laptop. The circuit schematic is shown in Fig. 4. A program is developed and loaded to the Arduino board that offers several actuation commands for the TCP<sub>FL</sub> and air pump. A software called processing <sup>3</sup> is used to send those commands to the Bluetooth module to activate the Arduino's uploaded code. Since the TCP actuators are high in resistance, they require voltages up to 50 V to perform at their optimal potential. Each TCP<sub>FL</sub> is connected to a boost converter, which works by increasing the battery voltage from 14.8 to 50 V. Each TCP<sub>FL</sub> in the joint has a resistance of  $R=250$  Ω and a length of 130 mm. As a result, with the 50 V provided from the battery, the output current across the resistance was  $I=0.2$  A. A 3 V micro-air pump was used to cool down the actuators after heating. This was done as a preliminary test, and we planned to do a systematic study on the cooling rate and effect in the actuators in the future. A voltage divider circuit was also created by using resistors (~97 Ω) to step down the battery's 14.8–3.6 V for the mini pump.

## Results and discussion

To validate the versatility of the multidirectional FGM joint, different experiments are performed. To start with, a relation between the bending angle and the input power

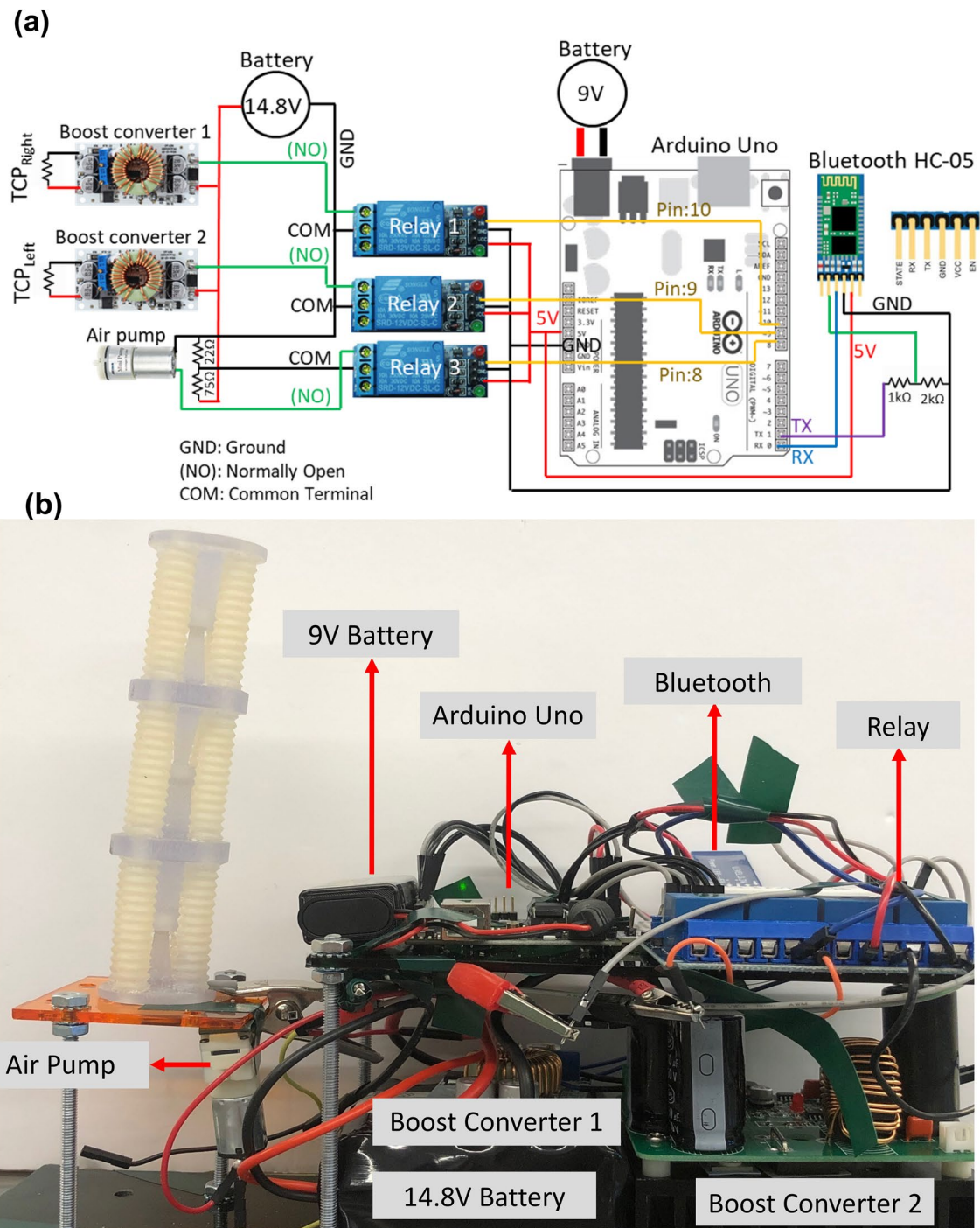


**Fig. 4** Developed circuit for wireless control of the multifunctional FG robot: **a** circuit diagram and **b** circuit setup

is studied. Figure 5a shows that the joint has the capability to bend to maximum  $40^\circ$  in different directions by providing 0.22 A input current for 15 s. It is also observed that actuating at lower input current (0.12 and 0.14 A), for longer heating time (30 s), the joint is still capable of reaching  $20^\circ$ – $35^\circ$  bending angle (Fig. 5a). Moreover, this

experiment confirmed that the 3D-printed FGM joint has a consistent stiffness gradient in all sides.

The relation between the input power and the maximum bending angle is presented in Fig. 5b. To achieve the maximum bending angle in each direction  $13.5$  W of power is required, while the required force is  $1.5$  N (Fig. 5c). However, by actuating the joint in opposite directions with the



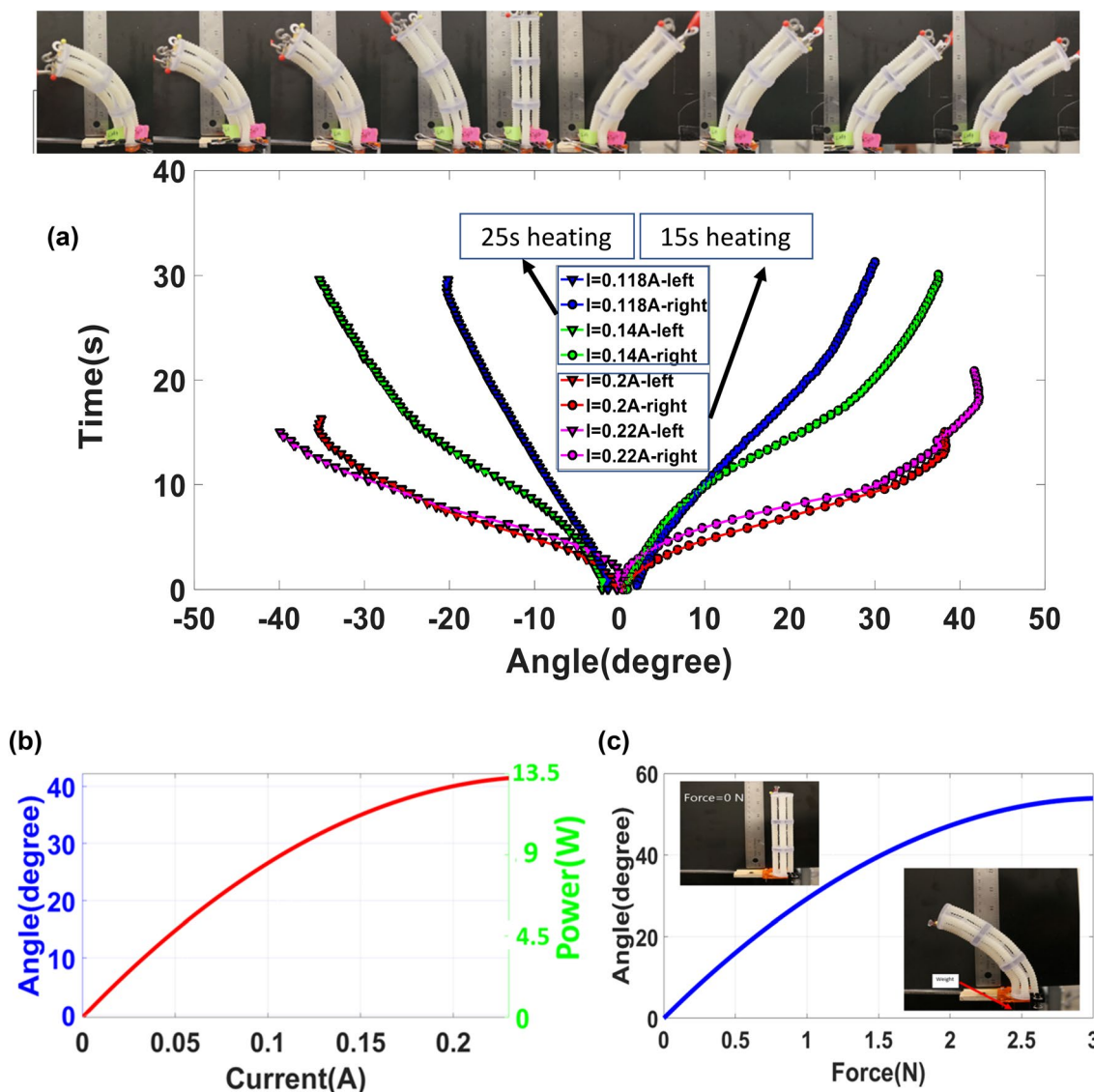


**Fig. 5** FGM joint actuation: **a** single actuation of the joint in left and right direction by increasing power from 0.11 to 0.22 A, **b** relation between actuation angle, current, and power for bending the FGM joint, and **c** relation between the required force and the bending angle

“ON/OFF” power sequence, a bending bias is observed which is the effect of insufficient cooling (due to the relatively high frequency of actuation). This is an undesired attribute for the various applications where the system will be deployed unless an air pump is included. As a result, developing a suitable sequential powering pattern can help the joint to bend smoothly and equally in both directions without the integration of an air pump. In sequential actuation, first, one of the actuators (the right TCP) is actuated using a two-stage heating pulse. Next, the opposite side (left TCP) is actuated immediately after the first actuator is turned off. This will bring back the structure to its original position. A similar process is followed to actuate the joint in the other direction. Figure 6a shows the actuator behavior

using the sequential powering conceived for bending in opposite directions. A similar trend is observed previously in actuator characterization (Fig. 3c-i, ii); the increase in the actuation strain and temperature will cause the joint to bend more effectively at a faster rate. Trajectory planning is an important aspect of the different applications for this structure. The joint is able to accommodate up to 4 TCPs, each located in its own confined channel. By actuating the 4 TCPs in a variation of sequences and times, we can control the bending of the joint. Although it is not the focus of this paper, trajectory planning is important for various applications. We have shown one example of the trajectory obtained by the proposed structure experimentally. Figure 6b shows the XY position plot of the joint with 4 muscles actuated to

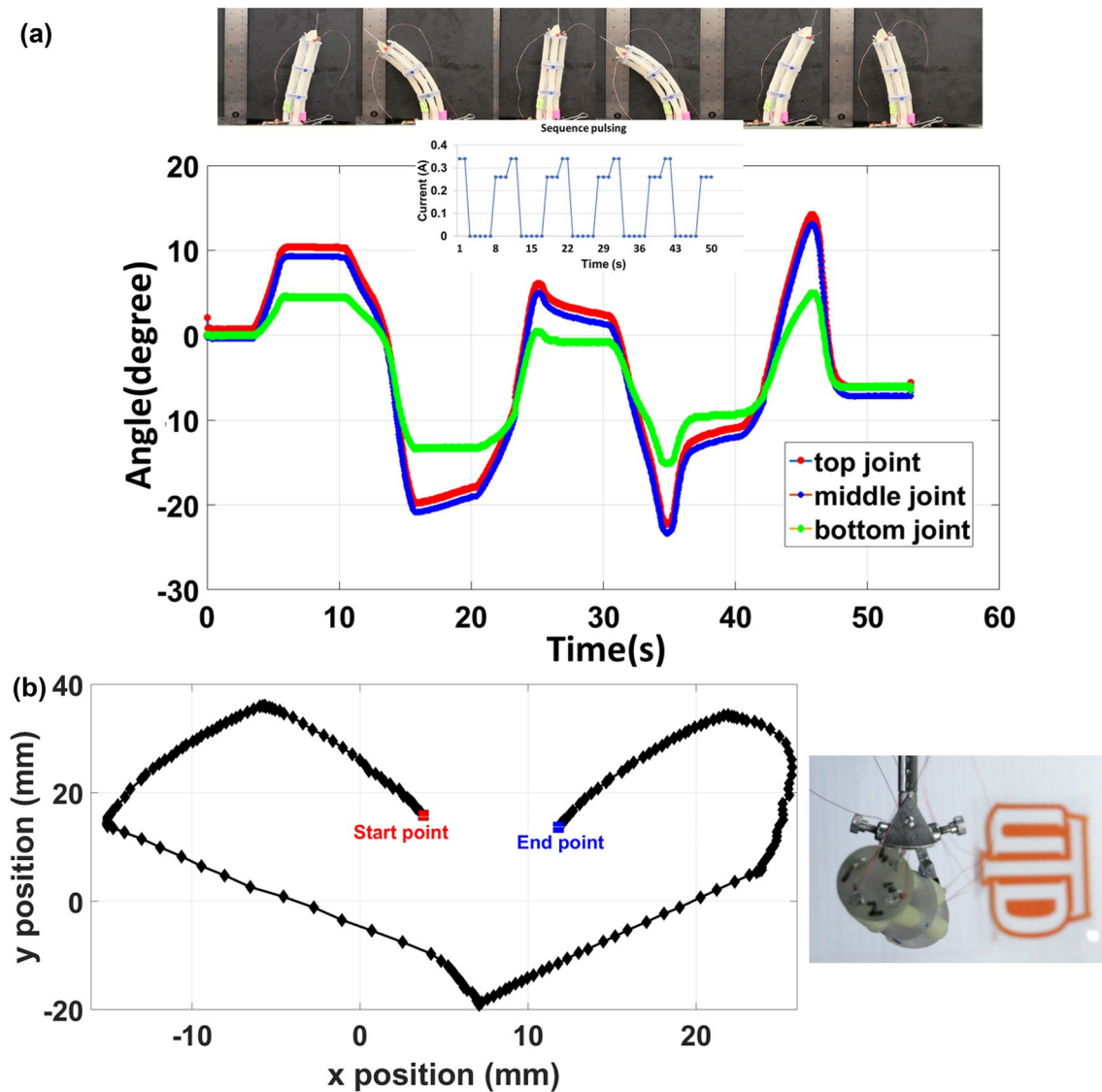


**Fig. 6** FGM joint actuation: **a** results of sequential powering of the joint for 3 continuous cycles and sequential powering pattern of fishing line TCP muscle for bending the joint to opposite directions simultaneously, **b** trajectory control of the joint in multidirections

move in a heart curved path (supporting video information is provided). A relationship can be found by developing position analysis theoretically, as explained in supplementary information in [22], and will be the main focus in future work.

Different modes of bending can also be achieved by fixing the joint at different points. For example, by leaving the structure on a flat surface and using sequential actuation with a high current of 0.2 A for 5 s and a lower current of 0.14 A for 10 s, the FGM joint is able to roll as shown in Fig. 7a (following the blue points until they placed under the structure after 40 s). Moreover, the gradient body stiffness helps produce biomimetic body curvatures as shown in Fig. 7b. The other applications of the joint can be for underwater swimming or wing flapping in the air (Fig. 7c).

These examples show that potential future applications of the functionally graded joint system are wide spread. We only demonstrated few of the usages in the laboratory settings. Invertebrate animals, commonly called worms, move in a wide range of ways across its length using muscle expansions and contractions [30]. Inspired by these animals and using TCPs as the actuator, a robotic structure is developed which can expand, contract, and crawl. This kind of motion helps the robot to operate in unstructured environments such as pipes maintenance and diagnostic, or for detection purposes by carrying sensors, cameras, and payloads in dangerous environments such as where there is uncontained gas or radioactivity risk. It can also be used for medical applications such as surgical robotic tools. These are some of the potential applications of such structures.

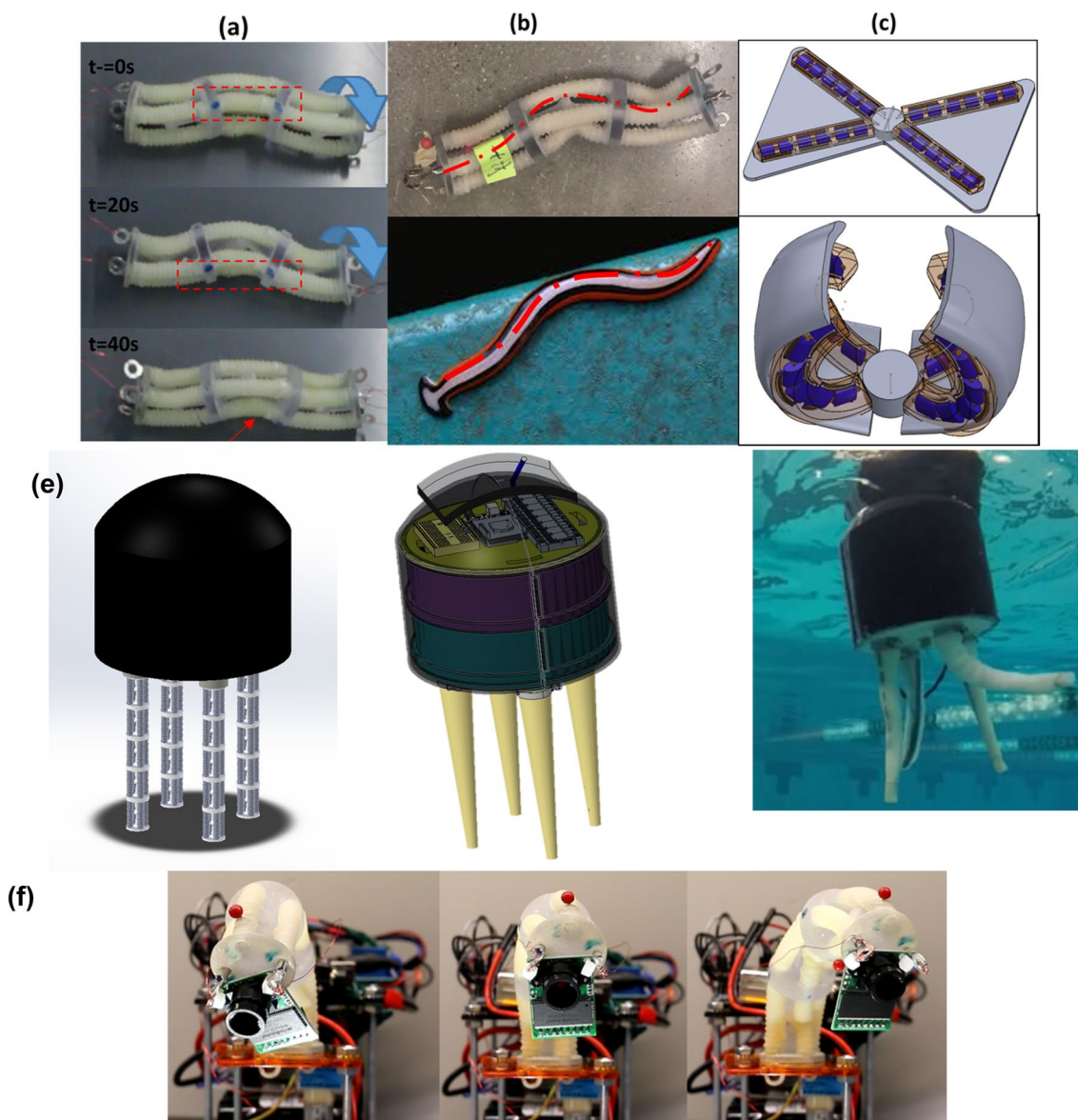


**Fig. 7** Different actuation modes and applications of soft modular joint: **a** crawling motion on a flat surface, **b** biomimicry body curvature, **c** future application in biomimetic wing, **e** application in octopus robot for grasping objects underwater, left new design with FGM arm

(left), CAD model of silicone arm made by casting silicone(middle), physical prototype of arm made by casting and testing in water (right) and **f** for monitoring and surveillance using the FGM structure and mounting a camera

Figure 7e shows the functionally graded joint integration as arms in a robotic octopus. Longer or shorter joints can be printed to accommodate the integration process or directly printed along with other structures. Unlike the soft silicone arms that have been presented in the octopus arm, the integration of the joint with 4 channels to embed the actuators adds more degrees of freedom to the arm bending. Above all, the functionally graded and the ability to print rubber-like structures solve the manufacturing problems of advanced bioinspired robots. Another application that is presented is the integration of a camera to the top section of the joint as shown in Fig. 7f. Here, the joint was able to position the

camera at different orientations due to the simulation of the actuators by the driving circuit discussed earlier. This shows that the system has great potential for monitoring and surveillance. Similar to the octopus, the system can be extended to be longer or shorter depending on the distance the camera needs to cover. Movie 1 shows a combined video summary of the bending achieved by the joint structure: first, a video with the cyclic actuation experiment presented in Fig. 5a; second, the rolling and multidirectional bending capabilities presented in Fig. 7a; third, a video highlighting the trajectory control presented in Fig. 6b; and lastly, a video presenting the joint in the bent position with a camera (arduinoCAM)

attached to the top section of the structure and the left and right TCP<sub>FL</sub> muscles actuated simultaneously, also shown in Fig. 7f. The camera is able to monitor up to 120° width (60° on each side). If the joint system is used for monitoring and surveillance, a quiet actuation system (silent actuation, without noise) such as the TCP<sub>FL</sub> actuators is essential for health operation. Other gear motors-based actuators or pneumatics are not good candidates for such applications.

## Conclusion

In this work, we have shown the fabrication, actuation principles, and functionality of a functionally graded modular joint actuated by TCP muscles. The idea of using cascaded joints in order to amplify movements of the end effector is investigated. Taking advantage of additive manufacturing technologies, the bending properties are controlled in the favorable direction within a complex 3D channel surrounding a rigid ball and socket joint. Stiffness gradient in the accordion-like channels improved the compliance of mimicking the biological systems. The most advanced fabrication, PolyJet technology was employed in single session printing to manufacture the joint. However, this method is expensive and still cannot reach the flexibility as the cast joint [30]. The channels are designed to keep the muscles inside, prevent heat loss when used in underwater, and increase the efficiency of the actuation. These channels are also necessary to keep the muscles safe in different environmental conditions such as underwater or cold aerial environments. Moreover, the fishing line TCP actuator (with nichrome wire as a heating element) is utilized for actuation, which worked very well in actuating the FGM joint. This polymer actuator resembles the tissue structure and can be easily contracted within the bioinspired systems. A complete characterization study of the TCP<sub>FL</sub> muscle under various input power parameters is performed and shown in Table 1 and Fig. 3. Later, the extracted data from the muscle characterization experiment are used to develop a sequential actuation pattern for the FGM joint to generate different curvatures. Finally, the FGM joint achieved untethered locomotion using the wireless circuit module. This circuit module is proposed for further development to control and advance the joint actuation. The optimized tether-less control can enhance the performances of the musculoskeletal joint to realize autonomous soft robot. All the presented performance features are highly desirable for the system operation in harsh environments. This class of FGM multidirectional robots will be well suited for real-world applications and tasks requiring continuous and dexterous deformation, while still having safe interaction with human and environments.

Future work will include varying the material properties further to match the desired attributes found in the molded

joints such as extremely elastic materials. Moreover, small PCBs and electronics hub will be designed to replace the circuit for direct integration in the body of the system. Studying path trajectory control such as feedback loop control based on the actuator properties (temperature, strain, and changes in the actuator resistance) will be developed for precise control and enhancement of the structure. We hope the results presented in this paper can serve as a benchmark for researchers who would like to explore similar works.

**Acknowledgements** The authors would like to acknowledge the support of the Office of Naval Research (ONR), Young Investigator Program, under Grant No. N00014-15-1-2503. We would also like to thank Farzad Karami for his contribution on the design of the cascaded joint. Thanks are due to Dr. Clark Meyer for his help in 3D-printing the cascaded FGM joint.

## Compliance with ethical standards

**Conflict of interest** The author declares that he has no conflict of interest.

**Ethical approval** No studies with human or animal subjects were conducted afresh by the author for inclusion in this review article.

## References

1. Bhavar V, Kattire P, Thakare S, Singh R (2017) A review on functionally gradient materials (FGMs) and their applications. In: IOP conference series: materials science and engineering. IOP Publishing, Bristol
2. Erdogan F (1995) Fracture mechanics of functionally graded materials. *Compos Eng* 5(7):753–770
3. Knoppers G, Gunnink J, Van Den Hout J, Van Wliet W (2005) The reality of functionally graded material products. In: Intelligent production machines and systems-First I\* PROMS virtual conference: proceedings and CD-ROM set, Elsevier, Amsterdam
4. Monzón M, Liu C, Ajami S, Oliveira M, Donate R, Ribeiro V, Reis RL (2018) Functionally graded additive manufacturing to achieve functionality specifications of osteochondral scaffolds. *Bio-Des Manuf* 1(1):69–75
5. Migliore SA, Brown EA, DeWeerth SP (2007) Novel nonlinear elastic actuators for passively controlling robotic joint compliance. *J Mech Des* 129(4):406–412
6. Zhang B, Luo Y, Ma L, Gao L, Li Y, Xue Q, Yang H, Cui Z (2018) 3D bioprinting: an emerging technology full of opportunities and challenges. *Bio-Des Manuf* 1(1):2–13
7. Ji K, Wang Y, Wei Q, Zhang K, Jiang A, Rao Y, Cai X (2018) Application of 3D printing technology in bone tissue engineering. *Bio-Des Manuf* 1(3):203–210
8. Richter C, Jentzsch S, Hostettler R, Garrido JA, Ros E, Knoll A, Rohrborn F, van der Smagt P, Conradt J (2016) Musculoskeletal robots: scalability in neural control. *IEEE Robot Autom Mag* 23(4):128–137
9. Mizuuchi I, Nakanishi Y, Sodeyama Y, Namiki Y, Nishino T, Muramatsu N, Urata J, Hongo K, Yoshikai T, Inaba M (2007) An advanced musculoskeletal humanoid kojiro. In: 2007 7th IEEE-RAS international conference on humanoid robots, IEEE

10. Kurumaya S, Suzumori K, Nabaie H, Wakimoto S (2016) Musculoskeletal lower-limb robot driven by multifilament muscles. *Robomech J* 3(1):18
11. Niiyama R, Nagakubo A, Kuniyoshi Y (2007) Mowgli: a bipedal jumping and landing robot with an artificial musculoskeletal system. In: *Proceedings 2007 IEEE international conference on robotics and automation, IEEE*
12. Niiyama R, Kuniyoshi Y (2010) Design principle based on maximum output force profile for a musculoskeletal robot. *Ind Robot Int J* 37(3):250–255
13. Ikemoto S, Kimoto Y, Hosoda K (2015) Shoulder complex linkage mechanism for humanlike musculoskeletal robot arms. *Bioinspiration Biomim* 10(6):066009
14. Tadesse Y, Wu L, Saharan LK (2016) Musculoskeletal system for bio-inspired robotic systems. *Mech Eng Mag Sel Artic* 138(03):S11–S16
15. Wu L, Tadesse Y (2016) Musculoskeletal system for bio-inspired robotic systems based on ball and socket joints. In: *ASME 2016 international mechanical engineering congress and exposition, American Society of Mechanical Engineers*
16. Robertson MA, Paik J (2017) New soft robots really suck: vacuum-powered systems empower diverse capabilities. *Sci Robot* 2(ARTICLE):eaan6357
17. Must I, Sinibaldi E, Mazzolai B (2019) A variable-stiffness tendril-like soft robot based on reversible osmotic actuation. *Nat Commun* 10(1):344
18. Karnati N, Kent BA, Engeberg ED (2013) Bioinspired sinusoidal finger joint synergies for a dexterous robotic hand to screw and unscrew objects with different diameters. *IEEE-ASME Trans Mechatron* 18(2):612–623
19. Ransley M, Smitham P, Miodownik M (2017) Active chain-mail fabrics for soft robotic applications. *Smart Mater Struct* 26(8):08LT02
20. Haines CS, Lima MD, Li N, Spinks GM, Foroughi J, Madden JD, Kim SH, Fang S, De Andrade MJ, Göktepe F (2014) Artificial muscles from fishing line and sewing thread. *Science* 343(6173):868–872
21. Almubarak Y, Tadesse Y (2017) Twisted and coiled polymer (TCP) muscles embedded in silicone elastomer for use in soft robot. *Int J Intell Robot Appl* 1(3):352–368
22. Wu L, Chauhan I, Tadesse Y (2018) A novel soft actuator for the musculoskeletal system. *Adv Mater Technol* 3(5):1700359
23. Tang XT, Li K, Liu YX, Zhou D, Zhao JG (2019) A soft crawling robot driven by single twisted and coiled actuator. *Sens Actuators Phys* 291:80–86
24. Tang X, Li K, Liu Y, Zhou D, Zhao J (2019) A general soft robot module driven by twisted and coiled actuators. *Smart Mater Struct* 28(3):035019. <https://iopscience.iop.org/article/10.1088/1361-665X/aaff2f/meta>
25. Yang Y, Li Y, Chen Y (2018) Principles and methods for stiffness modulation in soft robot design and development. *Bio-Des Manuf* 1(1):14–25
26. Bartlett NW, Tolley MT, Overvelde JTB, Weaver JC, Mosadegh B, Bertoldi K, Whitesides GM, Wood RJ (2015) A 3D-printed, functionally graded soft robot powered by combustion. *Science* 349(6244):161–165
27. Stratasys Ltd. 07/29/2019; Available from: <https://www.stratasys.com/materials/>
28. Mirzaali MJ, de la Nava AH, Gunashekar D, Nouri-Goushki M, Doubrovski E, Zadpoor AA (2019) Fracture behavior of bio-inspired functionally graded soft–hard composites made by multi-material 3D printing: the case of colinear cracks. *Materials* 12(17):2735
29. Salcedo E, Baek D, Berndt A, Ryu JE (2018) Simulation and validation of three dimension functionally graded materials by material jetting. *Addit Manuf* 22:351–359
30. Wu L, Karami F, Hamidi A, Tadesse Y (2018) Biorobotic systems design and development using TCP muscles. In: *Electroactive polymer actuators and devices (EAPAD) XX. International Society for Optics and Photonics*
31. LLC, m. Nichrome 70-30 Medium Temperature Resistor Material. [cited 2018; Available from: <http://www.matweb.com/search/DataSheet.aspx?MatGUID=70c6833687d54cb4a000bd49ffd8e86c&ckck=1>